A Hybrid Technique Based on Combining Ray Tracing and FDTD Methods for Site-Specific Modeling of Indoor Radio Wave Propagation

Ying Wang, Safieddin Safavi-Naeini, and Sujeet K. Chaudhuri, *Senior Member, IEEE*

***Abstract*—The paper presents a hybrid technique based on combining ray tracing and finite-difference time-domain (FDTD) methods for site-specific modeling of indoor radio wave propagation. Ray tracing is used to analyze wide area and FDTD is used to study areas close to complex discontinuities where ray-based solutions are not sufficiently accurate. The hybrid technique ensures improved accuracy and practicality in terms of computational resources at the same time since FDTD is only applied to a small portion of the entire modeling environment. Examples of applying the method for studying indoor structures and penetration of wave from outdoor to indoor are given at 2.4 GHz. Numerical results are compared with known exact solutions or results of the full wave analysis or traditional ray model to demonstrate the accuracy, efficiency, and robustness of the novel method. Numerical results are also compared with reported measurement results for waves at 1.29 GHz penetrating an external wall with metal-framed windows. Cumulative distributions of field envelope obtained from the hybrid method show close resemblance to the Rayleigh distribution, which conforms to the reported measurement results.**

***Index Terms*—Geometrical theory of diffraction, FDTD analysis, FDTD methods, indoor radio, ray tracing.**

I. Introduction

THE effective design, assessment, and installation of a radio network in an indoor environment require an accurate characterization of the radio propagation channel. Ray tracing technique has been demonstrated to be promising for indoor radio propagation modeling by many researchers [1]–[7]. The paths of radio wave propagation between the transmitter and the receiver are determined through transmission, reflection, and diffraction mechanisms. There are two general approaches employed to calculate these paths: imaging approach, which uses optical images of the transmitters and receiver [5]–[7] and ray-shooting technique [1]–[4]. Based on geometrical optics (GO) and usually supplemented with the uniform theory of diffraction (UTD), ray-tracing algorithm provides a relatively simple solution to indoor radio propagation. However, it is well known that GO provides good results for electrically large objects and UTD is rigorous only for perfectly conducting wedges. For complex lossy structures with finite dimensions encountered in indoor environment, ray tracing fails to predict correctly the scattered fields. In the complicated indoor communication environment, transmitting and receiving antennas are often inevitably installed close to these complex discontinuities, where no asymptotic solutions are available.

Such problem can be solved by numerical solution of the Maxwell's equations, in particular, the finite-difference time-domain (FDTD) method [8], [9]. By directly solving Maxwell's equations in the time domain, FDTD method fully accounts for the effects of reflection, diffraction, and radiation. The medium constitutive relation is automatically incorporated into the solution of Maxwell's equations. Therefore, it is well suited to study wave interactions in complex media. The advantages of the FDTD method are its accuracy and that it simultaneously provides a complete solution for all points in the map, which can give signal coverage information throughout a given area. However, as a numerical analysis method, FDTD method requires large amounts of memory to keep track of the solution at all locations, and extensive calculations to update the solution at successive instants of time. Application of accurate numerical analysis method to the entire modeling area is neither practical because of the computational resource required, nor is it necessary for open areas without many indoor objects. To the best of authors' knowledge, only limited numbers of reports exist on results for the indoor radio channel modeling using the FDTD method [10], [11].

Aiming at a cost-effective site-specific indoor radio channel model, in this paper, we present a hybrid technique based on combining ray tracing method with FDTD method for more accurate modeling of radio wave propagation. The basic idea is to use ray tracing to analyze wide areas and FDTD to study areas close to complex discontinuities, where ray-based solutions are not sufficiently accurate. FDTD is only applied to a small portion of the entire modeling environment, which ensures the practicality in terms of computational resources. The proposed hybrid method enables the study of effects of generic indoor structural features, furniture, inhomogeneity inside walls, and any objects that may have significant effect on signal coverage and statistics inside buildings. Signal intensity and phase at all points can be obtained in the FDTD computation domain, which provides information of both long-term shadowing effect and short-term fading effect. Therefore, besides path loss caused by the studied structure, probability distributions of the field envelope can be derived, which is needed for reliable design of radio communication system.

Combination of ray tracing and FDTD methods is described in detail in Section II. Applications of the proposed method for studying indoor structures and penetration of wave from outdoor to indoor are given at 2.4 GHz in Section III. Numerical

Manuscript received November 9, 1998; revised October 22, 1999.

The authors are with the Department of Electrical and Computer Engineering, University of Waterloo, Waterloo, ON, N2L 3G1, Canada.

Publisher Item Identifier S 0018-926X(00)04384-2.

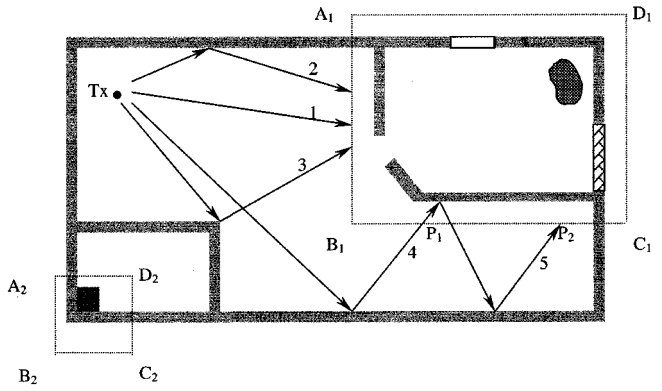

Fig. 1. An indoor environment with the interested areas enclosed by the virtual boxes $A_1B_1C_1D_1$ and $A_2B_2C_2D_2$. Different shades and textures are used to represent different building materials.

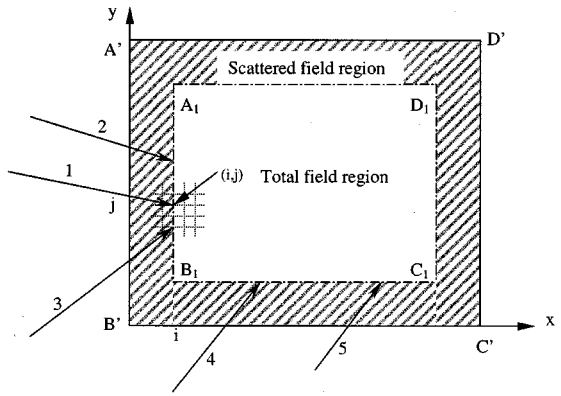

Fig. 2. Enlargement of the rectangle $A_1B_1C_1D_1$ in Fig. 1 showing the combination of ray-tracing and FDTD methods.

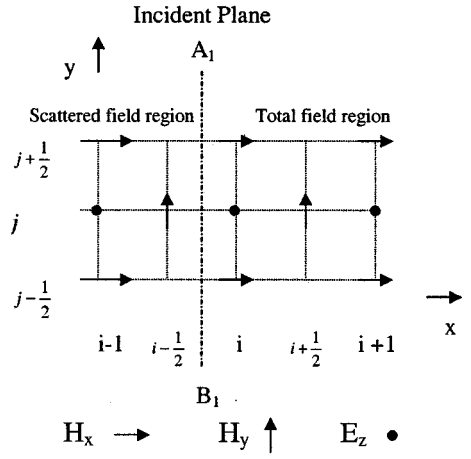

Fig. 3. Source excitation scheme.

results are presented and compared with known exact solutions, or results of the full wave analysis, or traditional ray model to demonstrate the accuracy, efficiency and robustness of our method. Numerical results are also compared with the measurement reported in [12] for waves at 1.29 GHz penetrating an external wall with metal-framed windows in Section III. Conclusions are given in the last section.

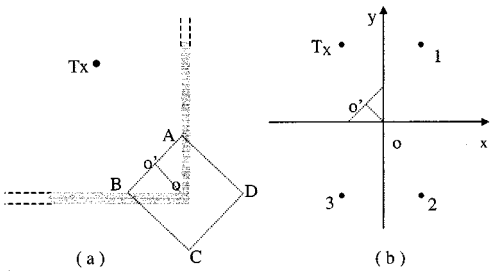

Fig. 4. The 2-D problem of a corner formed by two half-plane electric conductors. (a) An infinite electric line source located at T_X. (b) Equivalent sources.

II. Combination of Ray-Tracing and FDTD Methods

A. Ray-Tracing Method

The ray tracing is used first to cover the wide area with large scale and weak inhomogeneities. To this end, the ray-shooting technique is employed in this paper. However, with some modifications, the imaging approach of ray tracing is also applicable for the hybrid method.

Ray tubes are sent out from the transmitter. Each ray tube occupies a solid angle. The direction of each ray is determined by using the theory of geodesic domes [2] in three-dimensional (3-D) analysis, or by simply dividing the azimuth angle equally in two-dimensional (2-D) case. Objects are modeled as dielectric slabs with predefined thickness, boundaries, dielectric constant, and loss tangent, which is appropriate for most obstacles in indoor environments such as walls, ceiling, floors, windows, and doors. Reflection and transmission coefficients for lossy dielectric slabs are derived and given in [13].

The progress of each ray is traced throughout the environment. Starting from the source point, the algorithm follows the source ray direction and detects the closest object intersected by the ray. Once an intersection has been detected, the program generates one transmitted ray and one reflected ray. The reflected ray is stored and the transmitted ray is traced in a similar fashion to source rays. This continues until the ray intensity falls below a specified threshold or the ray exits the building. Next, a previously stored reflected ray is brought out and traced in the same way until all of the stored reflected rays are exhausted. The program then generates a new source ray from the transmitter. In the simulations in Section III, the ray termination threshold is defined with respect to the field strength at one wavelength from the transmitting antenna in free-space.

To determine the total field at a given point, a reception sphere is constructed around the receiving point with radius $r = \alpha d/\sqrt{3}$ [2] in 3-D case, where α is the angular spacing between neighboring rays at the source, d is the total path length traveled by the ray. In 2-D ray tracing, the radius is changed to $r = \alpha d/2$. If the ray intersects the reception sphere, it contributes to the total field at the receiving point. This criterion is used later in the next section to identify source rays entering the FDTD computation domain.

Diffraction is another propagation mechanism included in ray tracing. In indoor environment, most of the structures causing diffraction can be categorized into thick half plane such as doors, windows, and partitions, and right-angle wedge

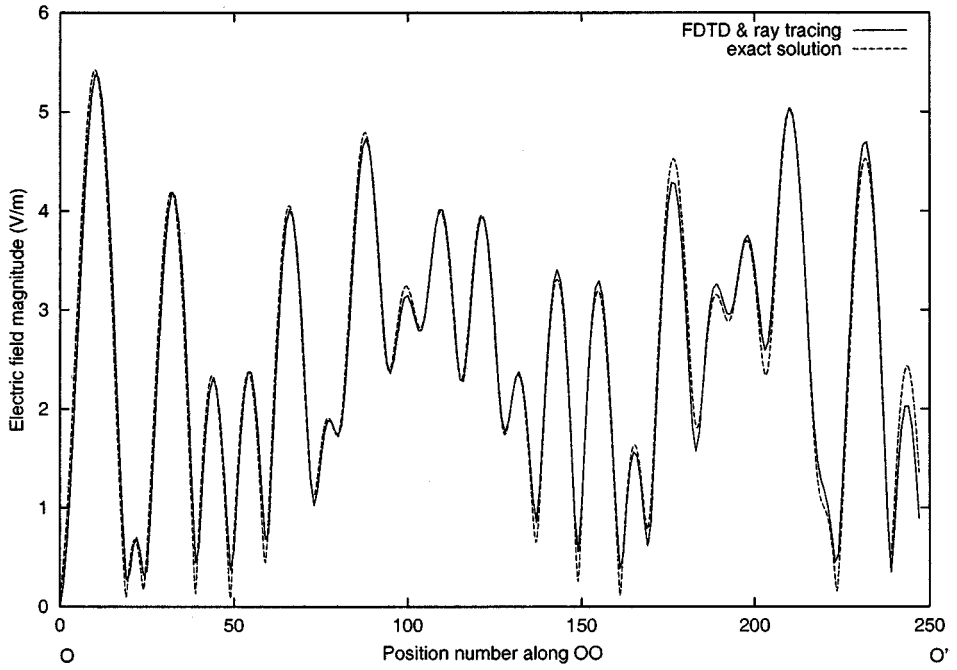

Fig. 5. Comparison of electric field distribution along OO' of Fig. 4 computed by the hybrid method and exact solution.

such as wall corner. To allow approximate treatment of lossy dielectric wedge diffraction, modified UTD [13] is used for the above two types of structures. When a diffracting edge is detected to be inside a ray tube, the ray tracing algorithm searches for any receiving points that have direct path to the diffracting edge. Diffracted field is then calculated and contributes to the total field at these receiving points. Diffracted rays are not traced further.

B. Combination with FDTD Method

In the next step, the region to be studied by FDTD method [8], [9] is enclosed by a virtual box. The region inside the virtual box may contain inhomogeneity in construction materials, isolated objects, or any structural features that are of interest. Surface sources exciting the field inside the virtual box are found by ray tracing. Whenever a ray tube intersects the box, the intersection position, ray direction, and electric field are stored in a data file, which is subsequently used in the FDTD method as the source excitation to analyze wave interaction with the structure enclosed in the box. Multiple virtual boxes can be defined so that source excitation into each enclosed region can be obtained after one execution of ray tracing. However, each region needs to be treated separately by FDTD afterwards. It is assumed that the receiving points of interest are in the enclosed regions.

As an example, Fig. 1 shows a 2-D environment with a transmitter T_x. An area of interest is enclosed by the dashed-line rectangle $A_1B_1C_1D_1$, which contains complex inhomogeneity while the rest of the area is quite open. The four sides of the rectangle are the incident planes providing interface between the intersecting rays and the FDTD method. Some typical rays that hit the rectangle are shown in Fig. 1, with ray 1 representing the direct ray, ray 2 reflected ray, and ray 3 diffracted ray. Inside the enclosed region, FDTD method will be used to fully account for the effects of reflection, diffraction, and scattering. Objects outside this region are treated by GO and modified UTD as explained in the ray-tracing part. Additional virtual boxes, e.g., $A_2B_2C_2D_2$, can be defined enclosing the square-shaped object

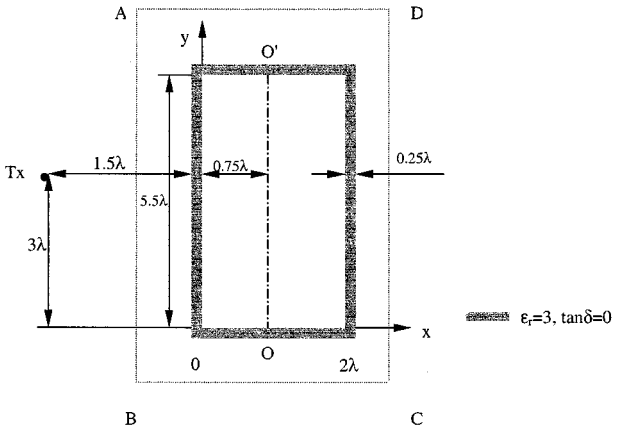

Fig. 6. Two-dimensional layout of a house with wooden walls and a transmitter located outside for studying penetration of wave from outdoor to indoor. The area of interest is enclosed by the virtual box $ABCD$.

TABLE I
COMPARISON OF RMS ERROR AND CPU TIME BY THE HYBRID METHOD AND RAY TRACING METHOD FOR THE CASE IN Fig. 6

	Hybrid method	Ray tracing method
rms. error (dB)	0.32	1.31
CPU time (S)	20	19

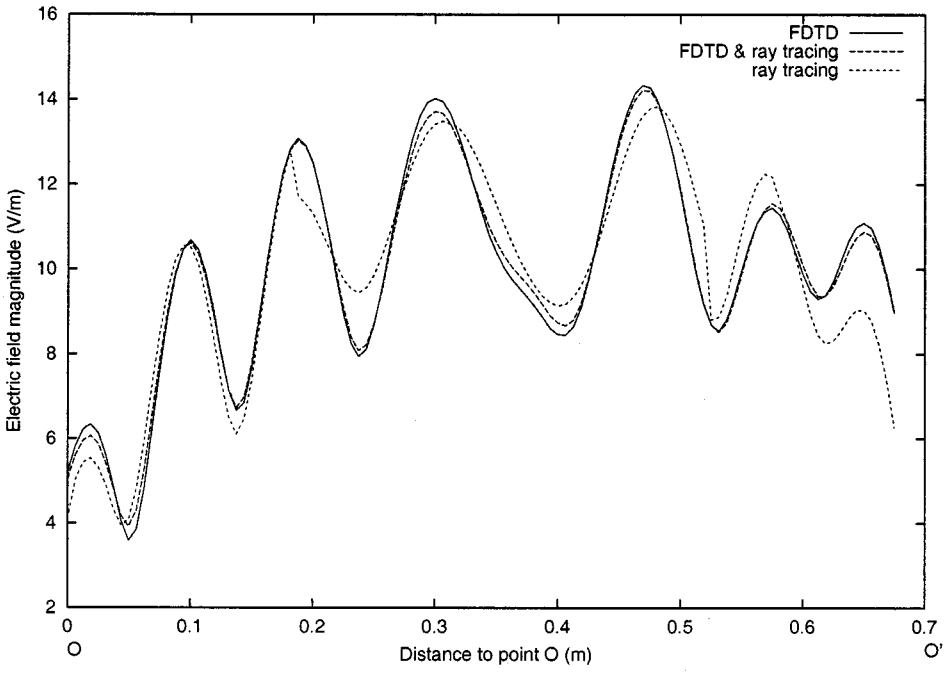

Fig. 7. Electric field distributions along OO' of Fig. 6.

at the left bottom corner if the field surrounding the object is also of interest.

Reflected or scattered field emerging from the virtual box will interact with the outside environment. Such high-order effects can be included using ray tracing when the interested area can still support well-defined rays such as the walls enclosed in $A_1B_1C_1D_1$ in Fig. 1. Ray 4 enters the enclosed area from point P_1 and reflected by a wall. If traced further, the reflected ray exits this area and after one more reflection, it re-enters the area as ray 5 at point P_2. Both ray 4 and ray 5 can be included in the subsequent FDTD computation to incorporate high-order ray effects.

The rectangle $A_1B_1C_1D_1$ in Fig. 1 is enlarged in Fig. 2 to demonstrate the FDTD grid. To simplify the explanation, TM polarization, which involves three field components: E_z, H_x and H_y, is assumed in what follows. Space increments of the FDTD grid in x and y directions are Δx and Δy, respectively. In order to generate the incident wave, we need to specify the exact field distribution on the incidence planes at each time interval. The field distribution is derived from previously stored intersecting rays. Consider node $(i,j)(x = i\Delta x, y = j\Delta y)$ in Fig. 2 on the incident plane A_1B_1. The distance from node (i,j) to each ray is evaluated. As stated earlier, if the distance between node (i,j) and a ray is less than $\alpha d/\sqrt{3}$ in 3-D or $\alpha d/2$ in 2-D case, node (i,j) is considered to be in the ray tube and the ray contributes to the total field at node (i,j). If k rays hit the node, the electric field at (i,j) becomes $\vec{E}(i,j) = \sum_{n=1}^{k} \vec{E}_n$, where $\vec{E}_n$ is the time dependent electric field of the nth ray at point (i,j). Also, adjacent nodes can be illuminated by the same ray as shown in Fig. 2: both node (i,j) and its adjacent nodes $(i,j-1)$ and $(i,j+1)$ can have contribution from ray tube 1.

The actual computation domain of FDTD extends to $A'B'C'D'$, which is larger than rectangle $A_1B_1C_1D_1$, as

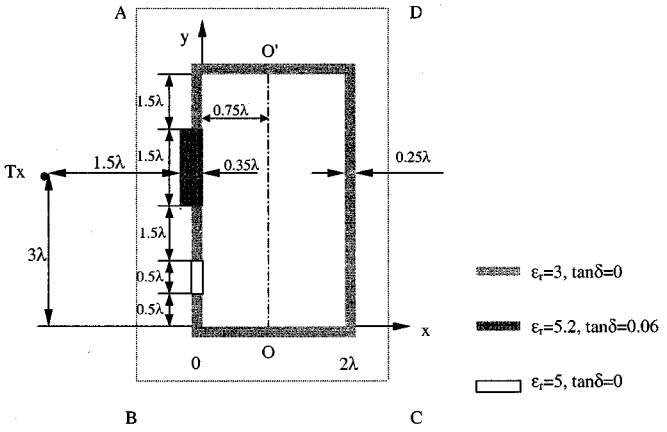

Fig. 8. Two-dimensional layout similar to Fig. 6 with the addition of a lossy door and a window.

shown in Fig. 2. The shaded area is the scattered-field region, which is introduced to reduce parasitic waves generated by the source excitation method described above [9]. The area inside is the total-field region. This approach is based on the decomposition of the electric and magnetic fields as

$$\vec{E}_{\rm tot} = \vec{E}_{\rm scat} + \vec{E}_{\rm inc}$$
$$\vec{H}_{\rm tot} = \vec{H}_{\rm scat} + \vec{H}_{\rm inc}$$

where subscriptions $\rm tot$, $\rm scat$, and $\rm inc$ are used to denote total, scattered, and incident components of electric and magnetic fields, respectively. In the scattered-field region, the algorithm only operates on scattered-field components, which implies that there is no incident wave in this region. In the total-field region, where the structure of interest is embedded, the algorithm operates on the total field. Incident wave is introduced

along the interface between these two regions. The source excitation scheme is demonstrated in Fig. 3, which shows field components around node (i,j) along incident plane A_1B_1. The evaluation of $E_z(i,j)$ at time step $(n+1)$, denoted by $E_z^{n+1}(i,j)$, using the FDTD propagator requires knowledge of the preceding half time step values of $H_y(i-1/2,j)$, $H_y(i+1/2,j)$, $H_x(i,j-1/2)$ and $H_x(i,j+1/2)$. There is inconsistency if the FDTD propagator is applied blindly, because $E_z(i,j)$, $H_y(i+1/2,j)$, $H_x(i,j-1/2)$ and $H_x(i,j+1/2)$ are in the total-field region while $H_y(i-1/2,j)$ is in the scattered field region. The correct equation for updating $E_z(i,j)$ is given by Taflove [8] as

$$\begin{aligned} E_{z,\mathrm{tot}}^{n+1}(i,j) &= E_{z,\mathrm{tot}}^{n}(i,j) + \frac{\Delta t}{\varepsilon_0 \Delta} \\ &\times \left[\begin{array}{l} H_{y,\mathrm{tot}}^{n+\frac{1}{2}}\left(i+\frac{1}{2},j\right) - H_{y,\mathrm{scat}}^{n+\frac{1}{2}}\left(i-\frac{1}{2},j\right) \\ +H_{x,\mathrm{tot}}^{n+\frac{1}{2}}\left(i,j-\frac{1}{2}\right) - H_{x,\mathrm{tot}}^{n+\frac{1}{2}}\left(i,j+\frac{1}{2}\right) \end{array} \right] \\ &- \frac{\Delta t}{\varepsilon_0 \Delta} H_{y,\mathrm{inc}}^{n+\frac{1}{2}}\left(i-\frac{1}{2},j\right) \end{aligned} \tag{1}$$

where Δt and Δ are time and space increments of the FDTD propagator and ε_0 is the permittivity of free-space. $\Delta x = \Delta y = \Delta$ is assumed for simplicity. Similarly, the scatter field of H_y at node $(i-1/2,j)$

$$\begin{aligned} H_{y,\mathrm{scat}}^{n+\frac{1}{2}}\left(i-\frac{1}{2},j\right) &= H_{z,\mathrm{scat}}^{n-\frac{1}{2}}\left(i-\frac{1}{2},j\right) + \frac{\Delta t}{\mu_0 \Delta} \\ &\times \left[E_{z,\mathrm{tot}}^{n}(i,j) - E_{z,\mathrm{scat}}^{n}(1-1,j)\right] \\ &- \frac{\Delta t}{\mu_0 \Delta} E_{z,\mathrm{inc}}^{n}(i,j) \end{aligned} \tag{2}$$

where μ_0 is the permeability of free space. Note that (1) and (2) are made consistent by adding the last term. Therefore, both $E_z(i,j)$ and $H_y(i-1/2,j)$ components of the incident wave are required. With known incident ray direction and electric field, the incident magnetic fields can be readily calculated using plane wave model. Source excitations along B_1C_1, C_1D_1 and D_1A_1 are carried out in a similar manner.

After specifying the incident field distribution on the incident planes, waves are propagated into the enclosed region by the FDTD propagator. The absorbing boundary condition [14] is applied to update fields at the four boundaries: $A'B'$, $B'C'$, $C'D'$ and $D'A'$ in Fig. 2. Thus, field distribution inside the region is obtained.

Location and size of each virtual box can be defined flexibly, depending on interest. An area enclosed in the box with a larger dimension requires more memory and CPU time. Since ray tracing treats areas outside the box, any scattering effects omitted by GO and the modified UTD can not be included in the field inside the box, which can be a cause of error. However, scattering by small inhomogeneities is usually local in nature. Therefore, the predicted field inside the box is more accurate when the box boundaries are positioned away from outside scatterers. A proper choice of the dimension and location of the virtual box requires a good understanding of wave propagation mechanisms.

Applications of the hybrid technique of combining ray tracing and FDTD methods to 2-D problems will be presented in the next section. Computations are done at 2.4 GHz except for the last example, which is calculated at 1.29 GHz.

III. Numerical Results

A. Comparison with Exact Solution

To validate the method proposed here, a 2-D problem shown in Fig. 4(a) was studied first. It is a corner formed by two half-plane electric conductors. An electric line source is located at about 50λ from the corner, where λ is wavelength of the incident electromagnetic (EM) wave. In this geometry, ray tracing treats the entire region except the vicinity of the corner. The area to be analyzed by FDTD is enclosed by the dashed-line rectangle. For such a simple structure, the exact electric field distribution can be obtained by using equivalent sources to replace the conductors [15] as shown in Fig. 4(b). Assuming the electric line source is $\hat{z}I_e$, located at $(-x,y)$, the equivalent source 1 is $-\hat{z}I_e$, located at (x,y), equivalent source 2 is $\hat{z}I_e$, located at $(x,-y)$ and equivalent source 3 is $-\hat{z}I_e$, located at $(-x,-y)$. The electric field along OO', which is 10λ long, can be conveniently derived from the four sources. Fig. 5 shows both the exact solution and the predicted electric field along OO' by the hybrid method, where a grid resolution (Δ) of 25 cells/λ is used in the FDTD computation. A good agreement between the two curves can be seen.

B. Penetration of Wave from Outdoor to Indoor

Fig. 6 shows an example of applying the method to study wave penetration from outdoor to indoor. A wooden house, with dielectric constant $\varepsilon_r = 3$ and $\tan\delta = 0$, is enclosed in the dashed-line rectangle $ABCD$. The transmitter is located outside of the house. Wave propagation from the transmitter to the rectangle $ABCD$ is simulated by ray tracing, and FDTD is applied inside $ABCD$. The size of the house is chosen to be just a few wavelengths, so that full wave analysis by using FDTD can be applied to the entire scenario to verify the proposed method. Electric field distribution inside the house is computed and compared by three methods: FDTD method, the proposed hybrid method and the traditional ray tracing method. In the first method, the entire region including the transmitter and the house is modeled by FDTD method. In both the second and the third methods, the ray tube angle α is set to be 0.5°. Rays are terminated after their intensity dropped 30 dB below the reference level as explained in the previous section, i.e., threshold is -30 dB. It is observed that with lower threshold, there is no notable change in the resulting field distribution. In both the first and the second methods, the FDTD grid resolution is set to be 20 cells/λ. The dimension of the house is $2\lambda \times 5.5\lambda$. Therefore, in total 4400 (40×110) locations inside the house are calculated by the hybrid method and the traditional ray-tracing method. Results by the FDTD method are used as reference. Root mean square (rms) errors of the

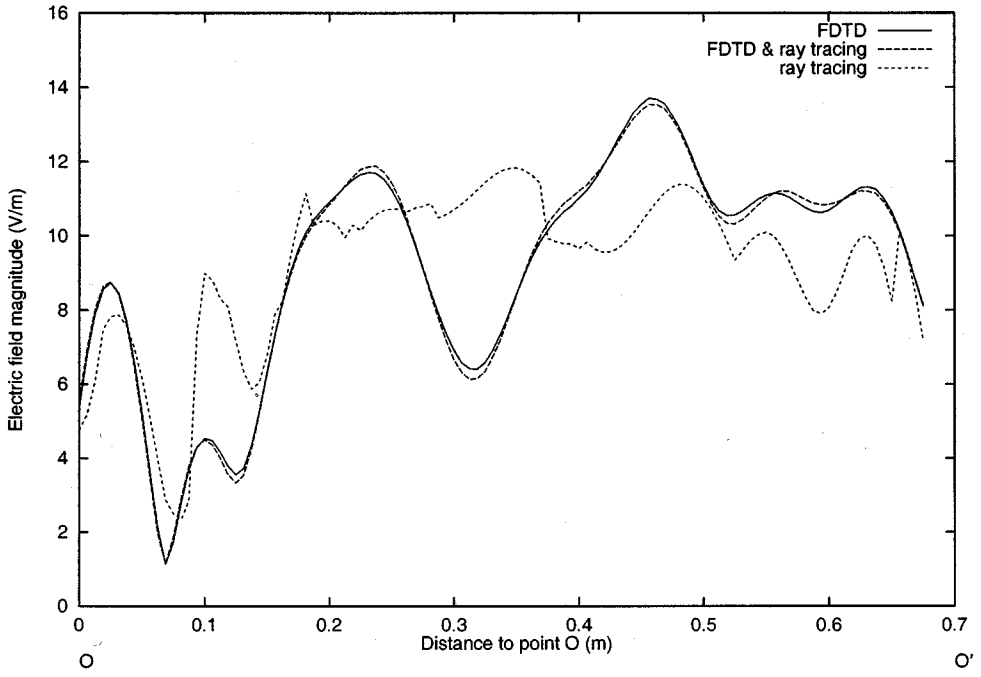

Fig. 9. Electric field distributions along OO' of Fig. 8.

other two methods and the computation CPU time on Pentium 450 are compared in Table I. In such a simple situation, both ray-tracing and the hybrid method give good results. It still can be seen that by including diffraction from corners, the hybrid method is more accurate than ray-tracing method. Fig. 7 shows electric field distribution along OO' of Fig. 6, which is 0.75λ away from the left wall.

Next, the situation in Fig. 6 is complicated by the presence of a lossy door with $\varepsilon_r = 5.2$ and $\tan\delta = 0.06$ and a window with $\varepsilon_r = 5$ and $\tan\delta = 0$, as shown in Fig. 8. The electric field distribution along OO' is shown in Fig. 9. It can be observed that the accuracy of ray tracing degrades compared to results shown in Fig. 7 for the simple case. Obviously, the inhomogeneity in the left wall plays an important role in this case, which is omitted in GO approximations. As shown in Table II, the rms error of ray tracing is increased by 1.81 dB. However, the hybrid method still shows good accuracy.

TABLE II
COMPARISON OF RMS ERROR AND CPU TIME BY THE HYBRID METHOD AND RAY TRACING METHOD FOR THE CASE IN Fig. 8

	Hybrid method	Ray tracing method
rms. error (dB)	0.29	3.12
CPU time (S)	20	19

C. Indoor Example

The next example studied is a two-room structure with the transmitter located in the left-side room, as shown in Fig. 10. The building material of the wall is assumed to have dielectric constant $\varepsilon_r = 8$ and $\tan\delta = 0.015$. A wall and a metallic door separate the two rooms. The structure of the left-side room is simple, hence, modeled by ray tracing. The right-side room has two windows and an open door, which is enclosed in the dashed-line rectangle $ABCD$ and is studied by FDTD. Results of the hybrid method are compared with those obtained by applying FDTD method to both rooms and those of the traditional ray-tracing method. In ray-tracing computations, the ray tube angle α is set to be 0.5° and threshold for ray termination is −30 dB. Beside reflections and transmissions, diffraction by the two diffracting edges E_1 and E_2 is also included in ray-tracing computations. In FDTD computations, the grid resolution is set to be 20 cells/λ. Both rooms are $4\lambda \times 5.5\lambda$ in size. Therefore,

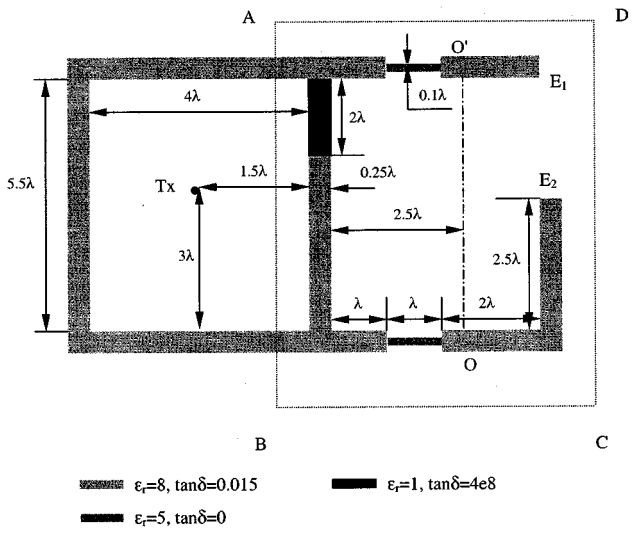

Fig. 10. Layout of a two-room indoor environment. The right-side room is enclosed in $ABCD$ and studied by FDTD.

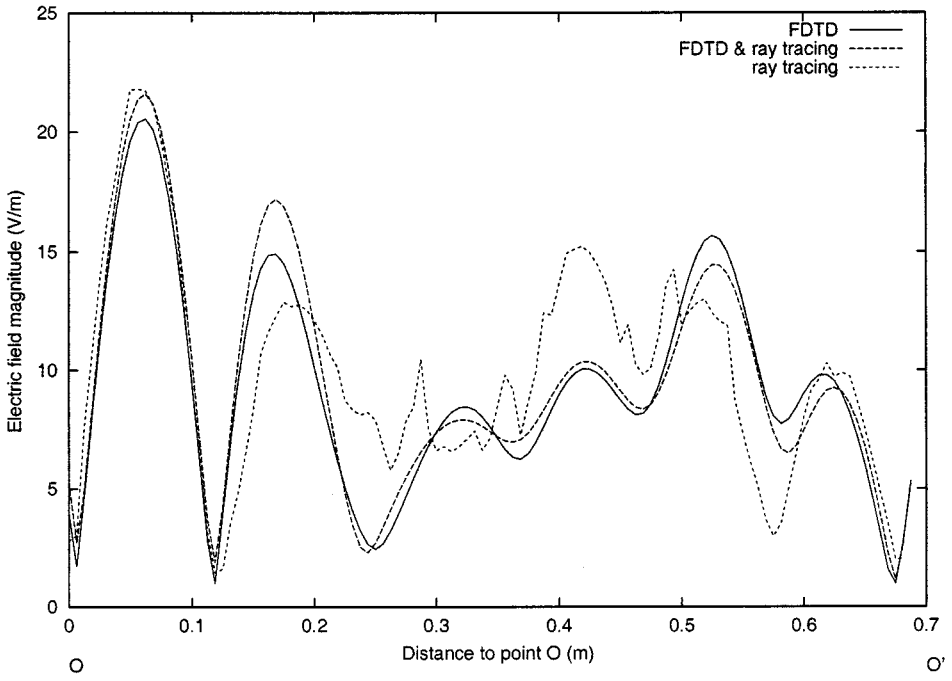

Fig. 11. Electric field distributions along OO' of Fig. 10.

8800 (80 $\times$ 110) locations inside the right-side room are calculated by the hybrid method and ray tracing method. Results by the FDTD method are used as reference. Table III compares the r.m.s. errors of ray tracing method and the hybrid method and CPU time on Pentium 450. It can be seen the accuracy is increased by about 2 dB by using the hybrid method. Fig. 11 shows electric field distributions along OO', which is arbitrarily chosen. A good agreement between the results by FDTD method and the results by the hybrid method can be observed. In this case the amount of CPU time needed by ray tracing is much more than the hybrid method, which is mainly because of the large number of computed receiving locations. Ray tracing is more efficient in terms of computation time if the number of receiving locations is less.

From the field distribution, one can obtain the probability distribution of field strength. Such statistical analysis gives information of probability of received signal level being above a threshold for good quality of service. First, from electric field distribution obtained by FDTD method, the average field power over the 8800 locations in the right-side room is calculated. Next field value at each location is normalized to the average power. The cumulative distribution of the normalized signal level is then computed and shown in Fig. 12 by the solid line. It can be read from Fig. 12 that 1% probability corresponds to -17 dB, which means that there is 1% probability that the received signal level is 17 dB below the average signal value. Field distributions obtained by ray tracing method and the hybrid method are processed in the same way and cumulative distributions are also shown in Fig. 12. As expected, the hybrid method provides an excellent estimation to the cumulative distribution of signal level.

TABLE III
COMPARISON OF RMS ERROR AND CPU TIME BY THE HYBRID METHOD AND RAY TRACING METHOD FOR THE CASE IN Fig. 10

	Hybrid method	Ray tracing method
rms. error (dB)	2.21	4.24
CPU time (M:S)	1:32	2:31

D. Effect of Ray Resolution

It is well known that a potential problem with ray tracing method is that it does not ensure that every signal path between the transmitter and receiver is considered, since it is impossible to send out infinite number of rays. The problem becomes more severe as the path length traveled by a ray from a source increases because of the spreading effect of the wave front of the ray tube and when the size of an object is small. The example shown in Fig. 13 is used to illustrate this problem, which shows a room, 10 m $\times$ 8 m in size, with an L-shaped structure at the left-bottom corner. Two adjacent rays are sent out from the transmitter and reflected by the wall. As shown in Fig. 13, the two reflected rays do not see the existence of the object at the corner. Were another ray sent out in between, the total field at some locations, especially in the vicinity of the object, would be very different. Such problem can be alleviated by using the hybrid method. The area close to the object is enclosed in the rectangle $ABCD$ in Fig. 13. Ray resolution becomes less of an issue where objects' size is large, such as the area outside of $ABCD$. Therefore, up to the incident plane of AD and CD, the

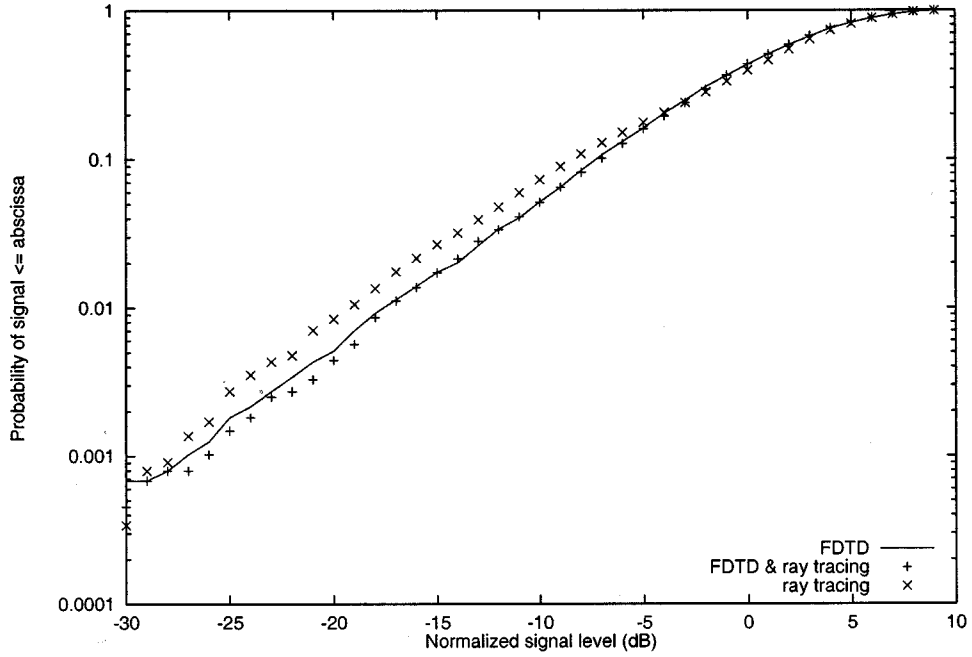

Fig. 12. The cumulative distribution of the normalized signal level in the right-side room of Fig. 10.

electric field distribution can be correctly determined, whether for a fine or a reasonably coarse ray resolution. Inside $ABCD$, any wave reflection or scattering is taken into account by FDTD.

The curves in Fig. 14 show the electric field distributions along OD computed by the hybrid method when ray tube angle $\alpha = 0.5°$ and $\alpha = 2°$. The two curves agree with each other quite well, which means same level of accuracy can be achieved with reduced number of rays. Fig. 15 compares electric field distributions along OD computed by the traditional ray-tracing method at different ray resolutions, where large difference can be observed especially at locations close to the object. This tends to indicate that the combined method is more robust than the ray-tracing method.

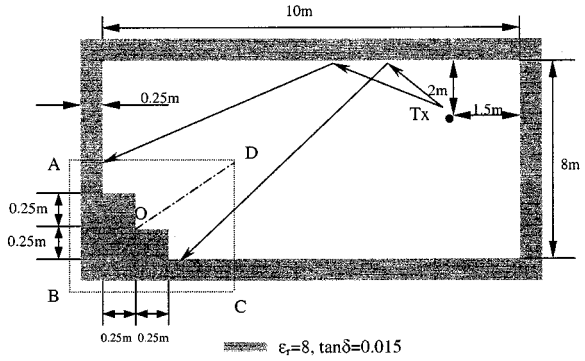

Fig. 13. A one-room structure with an L-shaped object at the left-bottom corner.

E. Comparison with Field Measurement

In this example, a comparison is made between simulation and measurement reported in [12] for wave penetration through an exterior wall at 1.29 GHz. Fig. 16 shows the side view and top view of the empty room where the measurement was taken. The exterior wall is covered with metal-framed window and three concrete posts that separate windows. All other sides are made of concrete walls and wooden doors. A vertically polarized Yagi array with 23 elements was used as the transmitting antenna, which is 888 m away from the exterior wall and wave incident angle is 3° off the wall surface normal as marked in the figure. The receiving antenna is standard dipole antenna. The measuring course O_1O_2 is parallel to the windows and 1 m away from the inner surface of the exterior wall, i.e., $d = 1$ m in Fig. 16. The measured signal envelope along O_1O_2 is shown in Fig. 17 [12] with an offset of -35 dB for clarity.

For this far-zone simulation, the problem is treated as 2-D and an electric line source is assumed as the transmitter. Both the traditional ray-tracing and the hybrid methods are used. The material properties and some structural dimensions are adopted from [3], where a comparison is made between ray-tracing simulation and the measurement results mentioned above. In the hybrid method, the rectangle $ABCD$ with a dimension of $75\lambda \times 9\lambda$ is drawn enclosing the exterior wall as shown in Fig. 16. Inside this area, the field distribution affected by metal-framed windows is obtained by FDTD method. In ray tracing computations, the ray tube angle α is set to be 0.01° in order to include the effect of concrete poles because of the large distance between transmitter and the room. Rays are terminated after their intensity dropped 40 dB below the reference level. In this case, the reference level is set to be the signal intensity at a location inside the room and right next to the window. Scattering effects of the window frames are not included in ray tracing computation. Simulation results are compared in Fig. 17, which have been normalized to the average signal level estimated from the measurement result. Reproduction of the measured signal en-

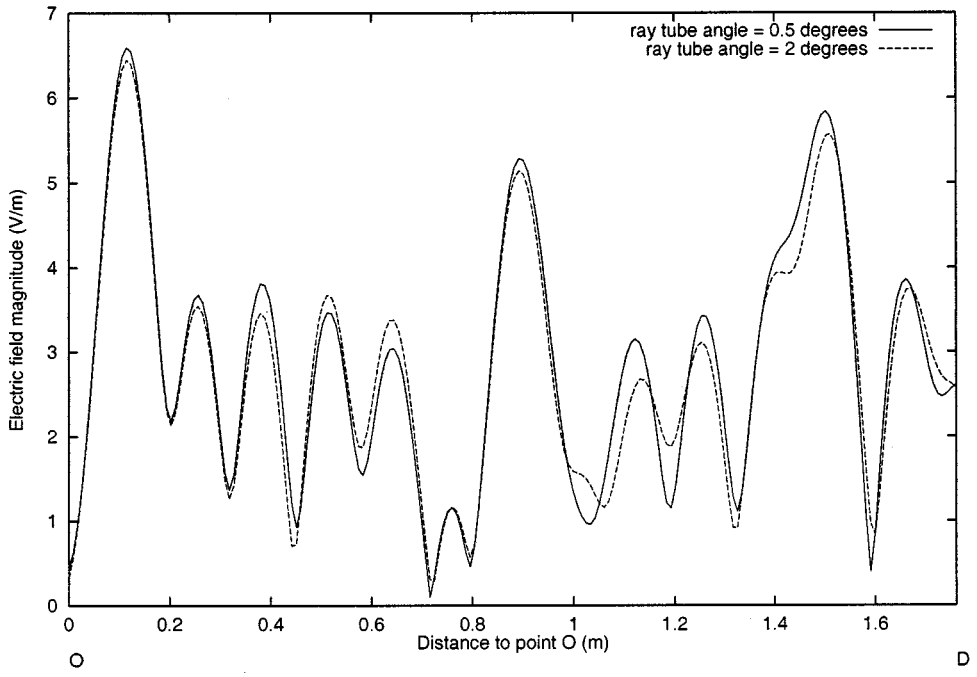

Fig. 14. Comparison of electric field distribution along OD of Fig. 13 computed by the hybrid method at different ray resolutions: $\alpha = 0.5^\circ$ and $\alpha = 2^\circ$.

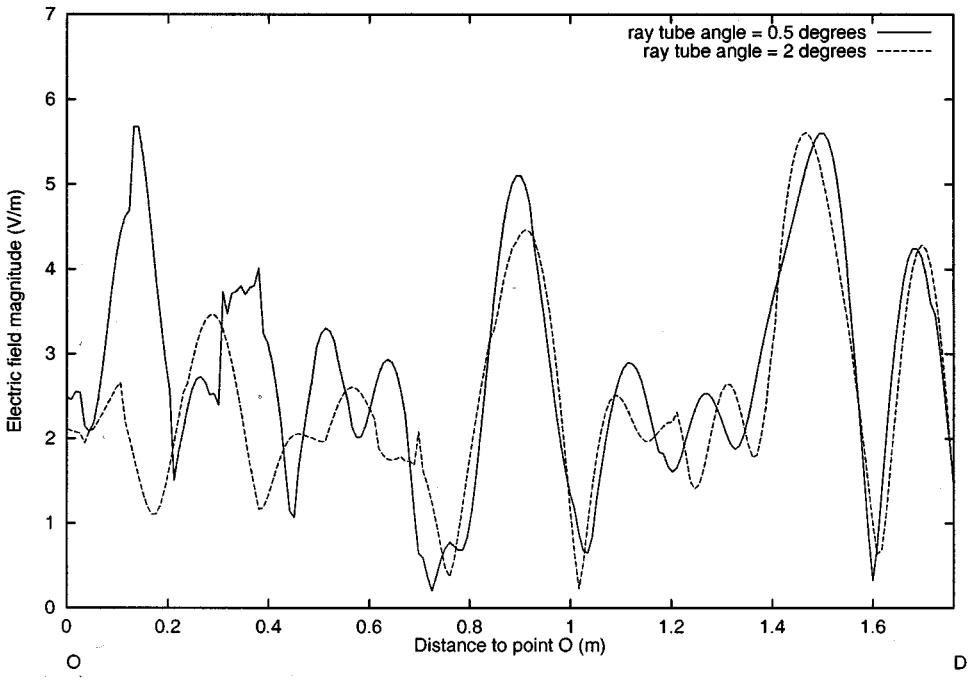

Fig. 15. Comparison of electric field distribution along OD of Fig. 13 computed by the traditional ray-tracing method at different ray resolutions: $\alpha = 0.5^\circ$ and $\alpha = 2^\circ$.

velope is impossible, since a lot of assumptions were made in the simulation due to the lack of accurate material and structural information, such as wall thickness, width of the metal frame, and dimensions of doors. However, as can be observed in Fig. 17, the results by the hybrid method accurately reproduce the fast fading phenomenon seen in the measured signal envelope and deep fades over 20–30 dB. The ray tracing results show a rather smooth variation along the measurement path similar to the simulation results reported in [3] because of GO approximation. The results in [3] show even less fluctuation than the ray tracing results in Fig. 17. Our speculation is that a higher threshold was used in [3], therefore, less numbers of reflections

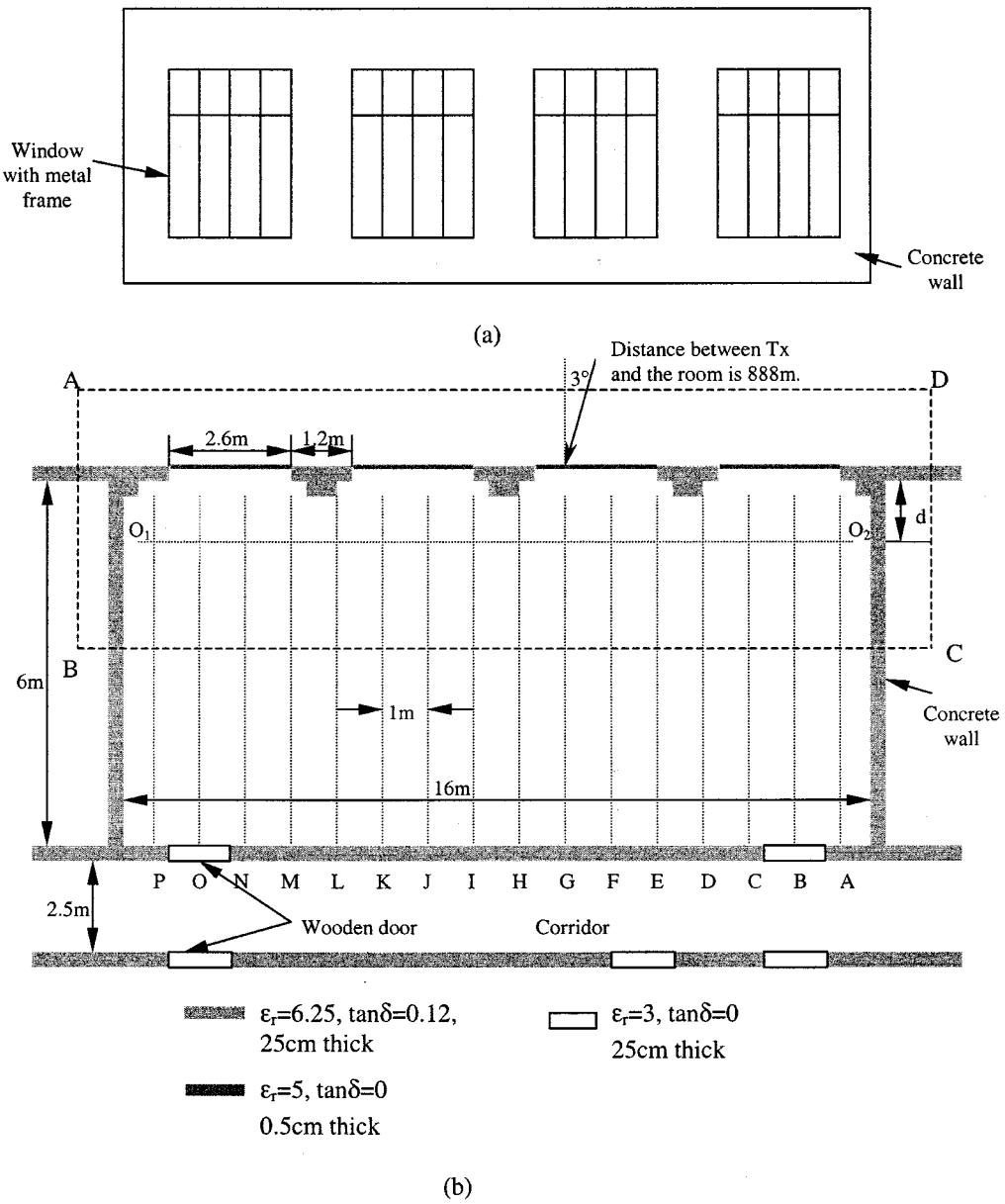

Fig. 16. (a) Side view and (b) top view of the room for simulation and measurement reported in [12] of wave penetration through an exterior wall at 1.29 GHz.

inside the room were considered. Both ray-tracing method and the hybrid method predict the excessive attenuation observed for signal envelope received near the poles.

Fig. 18 shows cumulative distributions of normalized signal level obtained from the hybrid method for two courses along O_1O_2 in Fig. 16 when $d = 4\lambda$ and $d = 5\lambda$. A close resemblance to the Rayleigh distribution can be observed, which conforms to the results derived from measurements in [12].

IV. Conclusion

A novel technique for site-specific modeling of indoor radio wave propagation is presented in this paper, which combines the strength of ray-tracing and FDTD methods. It has the flexibility of being able to be tailored to different environment according to desired accuracy. The FDTD module can be easily linked to existing ray-tracing procedure and disconnected for simple scenarios. Theoretically, the method can be applied to all frequency ranges of indoor communication. However, when frequency goes up, it becomes more demanding for computational resources to study common indoor structures with dimensions on the order of meters.

The proposed method provides a tool for studying effect of complex lossy structures encountered in indoor communication environment where no asymptotic solution is available. Results presented have demonstrated the accuracy and robustness of this technique. The proposed hybrid technique can generate very accurate and realistic simulated environment for predicting all relevant performance and "quality-of-service" parameters for various system architectures. Linking the present electromagnetic model, after some refinements, to system-level performance simulations is the next step in this research.

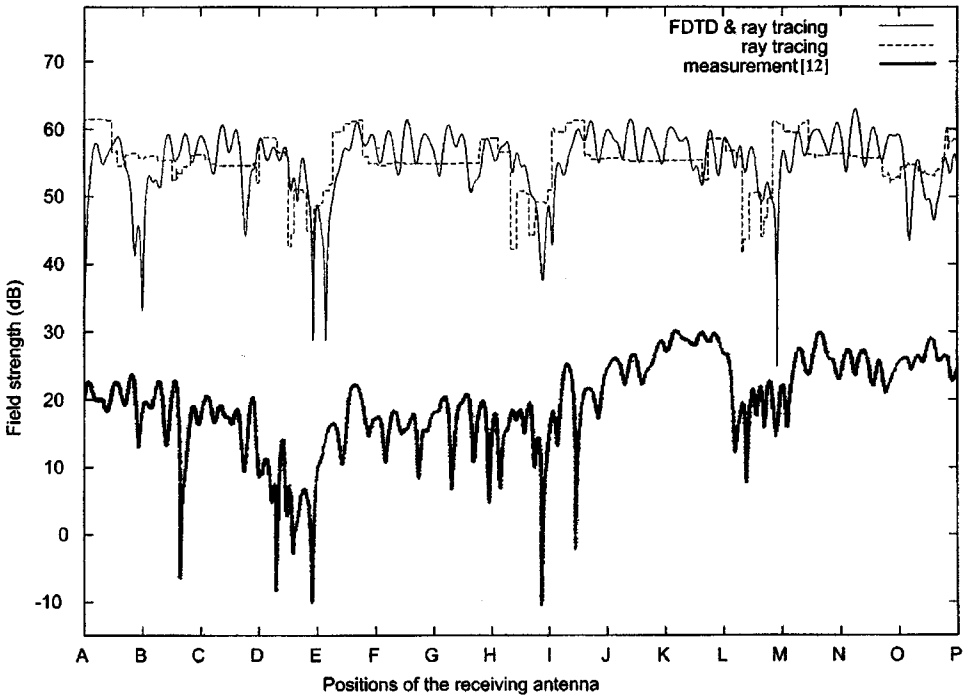

Fig. 17. Comparison of measured signal envelope along the measuring course O_1O_2 in Fig. 16 when $d = 1$ m [12] with simulation results by the hybrid method and ray-tracing method.

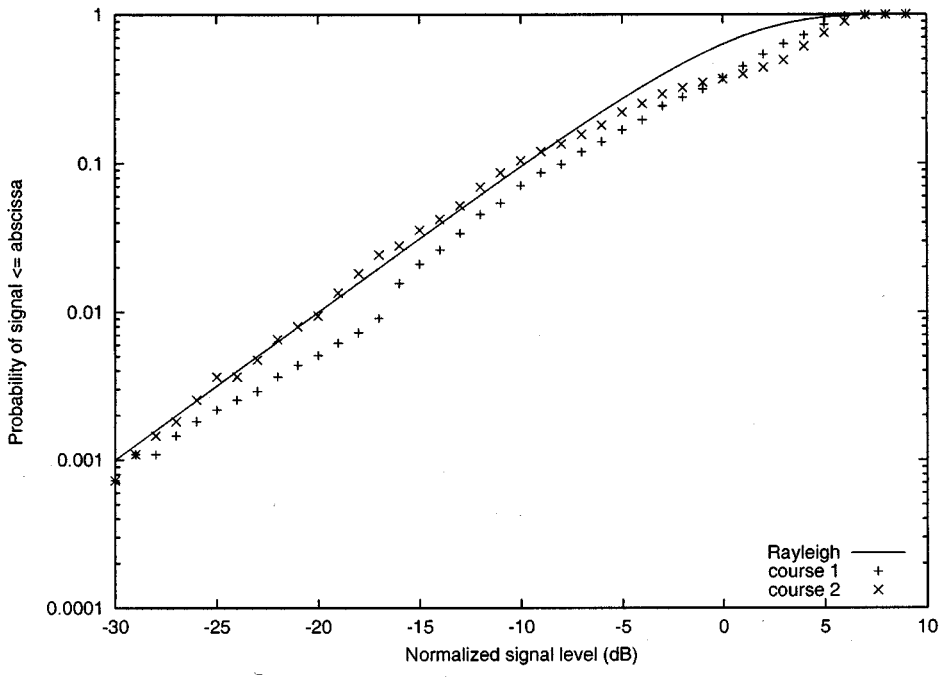

Fig. 18. Cumulative distributions of normalized signal level obtained from the hybrid method for two courses along O_1O_2 in Fig. 16 when $d = 4\lambda$ (course 1) and $d = 5\lambda$ (course 2).

REFERENCES

[1] G. Yang, K. Pahlavan, and J. F. Lee, "A 3-D propagation model with polarization characteristics in indoor radio channels," in *Proc. IEEE Globecom'93*, Houston, TX, Nov. 1993, pp. 1252–1256.

[2] S. Y. Seidel and T. S. Rappaport, "Site-specific propagation prediction for wireless in-building personal communication system design," *IEEE Trans. Veh. Technol.*, vol. 43, pp. 879–891, Nov. 1994.

[3] C. Yang, B. Wu, and C. Ko, "A ray-tracing method for modeling indoor wave propagation and penetration," *IEEE Trans. Antennas Propagat.*, vol. 46, pp. 907–919, June 1998.

[4] J. H. Tarng, W. R. Chang, and B. J. Hsu, "Three-dimensional modeling of 900-MHz and 2.44-GHz radio propagation in corridors," *IEEE Trans. Veh. Technol.*, vol. 46, pp. 519–527, May 1997.

[5] C. M. P. Ho and T. S. Rappaport, "Wireless channel prediction in a modern office building using an image-based ray tracing method," in *Proc. IEEE Globecom'93*, Houston, TX, Nov. 1993, pp. 1247–1251.
[6] J. W. Mckown and R. L. Hamilton, Jr., "Ray tracing as a design tool for radio networks," *IEEE Network Mag.*, vol. 5, no. 6, pp. 27–30, Nov. 1991.
[7] A. J. Rustako Jr., N. Amitay, G. J. Owens, and R. S. Roman, "Radio propagation at microwave frequencies for line-of-sight microcellular mobile and personal communications," *IEEE Trans. Veh. Technol.*, vol. 40, pp. 203–210, Feb. 1991.
[8] A. Taflove, *Computational Electrodynamics: The Finite-Difference Time-Domain Method*. Norwood, MA: Artech House, 1995.
[9] S. T. Chu, W. P. Huang, and S. K. Chaudhuri, "Simulation and analysis of waveguide based optical integrated circuits," *Comput. Phys. Commun.*, vol. 68, no. 1–3, pp. 451–484, 1991.
[10] K. Pahlavan and A. H. Levesque, "Wireless information networks," in *Wiley Series in Telecommunications and Signal Processing*. New York: Wiley, 1995, pp. 195–196.
[11] J. W. H. Lee and A. K. Y. Lai, "FDTD analysis of indoor radio propagation," in *IEEE Antennas Propagat. Soc. Int. Symp.*, vol. 3, Atlanta, GA, June 1998, pp. 1664–1667.
[12] J. Horikoshi, K. Tanaka, and T. Morinaga, "1.2 GHz band wave propagation measurements in concrete building for indoor radio communications," *IEEE Trans. Veh. Technol.*, vol. VT-35, pp. 146–152, Nov. 1986.
[13] Y. Wang, S. Safavi-Naeini, and S. K. Chaudhuri, "Comparative study of lossy dielectric wedge diffraction for radio wave propagation modeling using UTD and FDTD," in *IEEE Antennas Propagat. Soc. Int. Symp.*, vol. 4, Orlando, FL, July 1999, pp. 2826–2829.
[14] G. Mur, "Absorbing boundary conditions for the finite-difference approximation of the time-domain electromagnetic field equation," *IEEE Trans. Electromagn. Compat.*, vol. EMC-23, pp. 377–382, 1981.
[15] C. A. Balanis, *Advanced Engineering Electromagnetics*: Wiley, 1989.

Ying Wang received the B.Eng. and M.Eng. degrees in electrical engineering from Nanjing University of Science and Technology, Nanjing, China, in 1993 and 1996, respectively. She is currently working toward the Ph.D. degree in the Department of Electrical and Computer Engineering, University of Waterloo, Waterloo, ON, Canada.

Her research interests include numerical methods in electromagnetics and radio propagation modeling for indoor and microcellular communications.

Safieddin Safavi-Naeini was born in Gachsaran, Iran, in 1951. He received the B.Sc. degree in electrical engineering from the University of Tehran, Iran, in 1974, and the M.Sc. and Ph.D. degrees in electrical engineering, both from University of Illinois at Urbana-Champaign, in 1975 and 1979, respectively.

He joined the Electrical Engineering Department, University of Tehran, as an Assistant Professor in 1980 and became an Associate Professor in 1988. He has been an Associate Professor at the Electrical and Computer Engineering Department, University of Waterloo, since 1996. He has been a Scientific and Technical Consultant to a number of national and international telecom industrial and research organizations since 1980. His research interests and activities include numerical electromagnetics applied to RF/microwave/millimeter wave systems and circuits, antenna and propagation, wireless communication systems, very high-speed digital circuits, and optical communication systems.

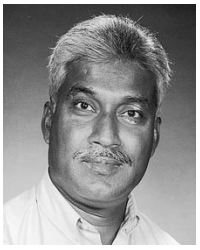

Sujeet K. Chaudhuri (M'79–SM'85) was born in Calcutta, India, on August 25, 1949. He received the B.E. (honors) degree in electronic engineering from BITS/Pilani, India, the M.Tech. degree in electrical communication engineering from IIT/Delhi, India, in 1970 and 1972, respectively, and the M.A.Sc. (microwave engineering) and Ph.D. (electromagnetic theory) degrees from the University of Manitoba, Canada, in 1973 and 1977, respectively.

In 1977, he joined the University of Waterloo, where he is currently a Professor in the Electrical and Computer Engineering Department and the Dean of the Faculty of Engineering. He has also held a Visiting Associate Professor's position in the EECS Department, University of Illinois at Chicago, during the years 1981 and 1984, a Visiting Professorship at the National University of Singapore from 1990 to 1991, and an Erskine Fellowship to the University of Canterbury, New Zealand, in 1998. He has been involved in contract research and consulting work with several Canadian and U.S. industries and government research organizations. His current research interests are in guided wave/electro-optic structures, planar microwave structures, dielectric resonators, optical and electromagnetic imaging, and the fiber-based broad-band network.

Dr. Chaudhuri is a member of URSI Commission B, and Sigma Xi.